



## Mineral paragenesis and textures associated with sandstone-hosted roll-front uranium deposits, NW China

Maozhong Min<sup>a,\*</sup>, Jia Chen<sup>b</sup>, Jinpeng Wang<sup>c</sup>, Guanhui Wei<sup>c</sup>, Mostafa Fayek<sup>d</sup>

<sup>a</sup>*Department of Earth Sciences, State Key Laboratory of Mineral Deposit Research, Nanjing University, Nanjing 210093, People's Republic of China*

<sup>b</sup>*State Key Laboratory of Solid State Microstructures, Nanjing University, Nanjing 210093, People's Republic of China*

<sup>c</sup>*Northwest Institute of Uranium Geology, China National Nuclear Corporation, Xianyang 712000, People's Republic of China*

<sup>d</sup>*Department of Earth and Planetary Sciences, University of Tennessee/ORNL, TN 37996, United States of America*

Received 28 April 2003; accepted 22 October 2004

Available online 28 January 2005

### Abstract

We present a first paragenetic study of the Wuyier, Wuyisan, Wuyiyi and Shihongtan sandstone-hosted roll-front uranium deposits, northwest China. The mineralization is hosted by Lower–Middle Jurassic coarse- to medium-grained sandstones, which are dark-gray to black due to a mixture of ore minerals and carbonaceous debris. The sandstone is alluvial fan-braided river facies. Minerals associated with these deposits can be broadly categorized as detrital, authigenic, and ore-stage mineralization. Ore minerals consist of uraninite and coffinite. This is the first noted occurrence of coffinite in this type of deposit in China. Sulfide minerals associated with the uranium minerals are pyrite, marcasite, and less commonly, sphalerite and galena. The sulfide minerals are largely in textural equilibrium with the uranium minerals. However, these sulfide minerals occasionally appear to predate, as well as postdate, the uranium minerals. This implies that there are multiple generations of sulfides associated with these deposits. The ore minerals occur interstitially between fossilized wood cells in the sandstones as well as replace fossilized wood and biotite. The deposits are generally low-grade. Primary uranium minerals associated with the low-grade deposits are generally too small, ranging from 0.2 to 0.3  $\mu\text{m}$  in diameter, to be observed by optical microscopy and are only observed by electron microscopy. Mineral paragenesis and textures indicate that these deposits formed under low temperature (30–50 °C) conditions.

© 2004 Elsevier B.V. All rights reserved.

*Keywords:* Sandstone-hosted roll-type uranium deposit; Mineralogy; Paragenesis; China

### 1. Introduction

Sandstone-hosted roll-front uranium deposits occur on nearly every continent and are an economically a significant source of uranium throughout the world. Examples include the Colorado Plateau, the Tertiary

\* Corresponding author.

E-mail address: [mzmin@nju.edu.cn](mailto:mzmin@nju.edu.cn) (M. Min).

Basin of Wyoming and the Ambrosia Lake of New Mexico, USA (Granger et al., 1961; Adler, 1964; Melin, 1964; Shawe and Granger, 1965; Dahl and Hagmaier, 1974), East Kalkarod, Goulds Dam, Honey-moon and Manyingee, Australia (IAEA, 1996), the Irkol, Kanzhugan, KyzYLtu, Mynkuduk and Uvanas, areas of Kazakhstan, Folakara, Madagascar, the area of La Sierrita, Mexico, and the Agron, Aktau, Bukeenai and Uchkuduk areas of Uzbekistan (Shawe and Granger, 1965; IAEA, 1996). In the early 1990s, a group of sandstone-hosted roll-front U-deposits, comprising two large and two medium tonnage deposits, were discovered in Xinjiang, Northwest China (216 Geological Party, 1997). These deposits are currently

being mined using an underground leaching technique and remain an important U source in China. This type of deposit also occurs in the northeast China–Inner Mongolia U-province, NE China (Chen et al., 2000).

Three of the four deposits occurring within the Xinjiang uranium province, Wuyier, Wuyisan and Wuyiyi, are located close to the borders of Xinjiang and Kazakhstan. The fourth, Shihongtan, is situated approximately 200 km SE of Ürümqi City (Fig. 1). Although these deposits have been mined for over a decade, very little is known about their genesis. The objectives of our study were therefore to document the mineral paragenesis and textures, and provide a simplified genetic model.

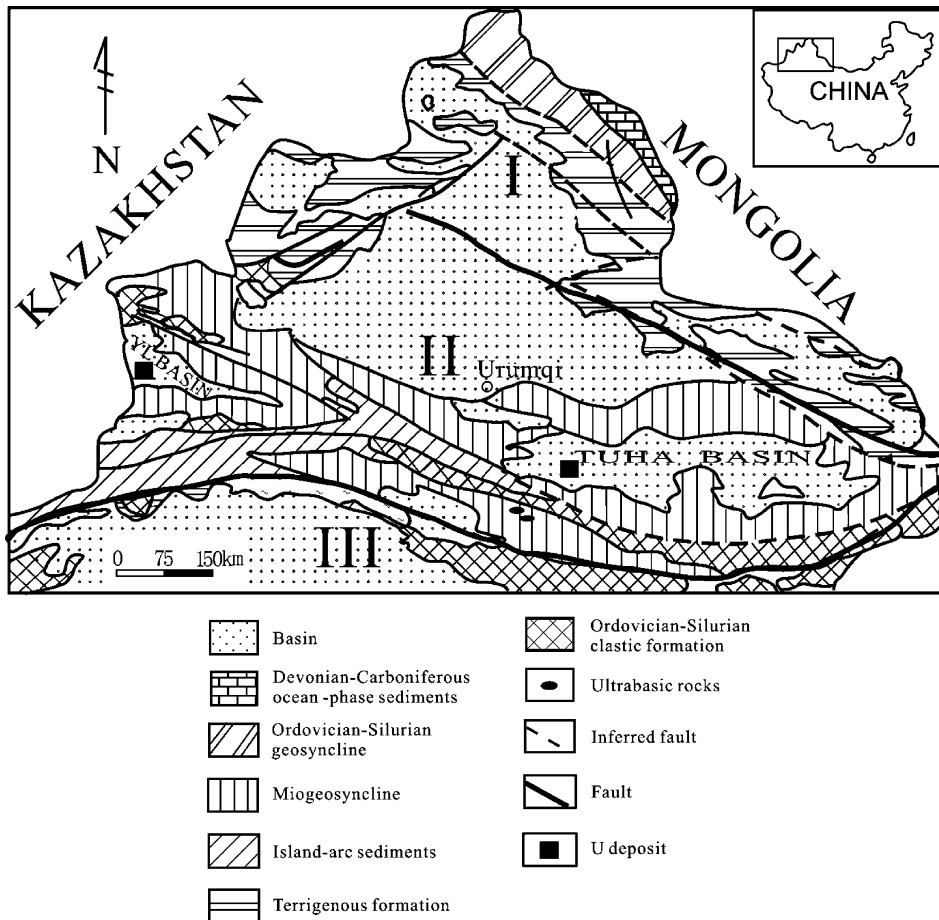


Fig. 1. Regional geological setting of NW China and geographical locations of the YL Basin, which hosts the Wuyier, Wuyisan, and Wuyiyi deposits, and the Tuha Basin, which hosts the Shihongtan deposit (modified after Chen, 1994). I—Xiboliya Plate; II—Kazakhstan Plate; III—Talimu Plate.

## 2. Geologic setting

The Wuyier, Wuyisan, Wuyiyi, and Shihongtan sandstone-hosted roll-front deposits occur in the Xinjiang U-province, NW China, the eastern extension of the Kazakhstan–Uzbekistan U-province (Chen et al., 2000). The Xinjiang province is currently one of the major regions for U exploitation in China. The

Wuyier, Wuyisan, and Wuyiyi deposits occur in the YL Basin with an area of approximately 16,000 km<sup>2</sup>. The Shihongtan deposit occurs within the Tuha Basin, which covers an area of about 51,000 km<sup>2</sup> (Figs. 1 and 2). These two basins are among seven basins located within the Tianshang Orogenic Belt, which occurs between the Xiboliya, Kazakhstan and Talimu tectonic plates. NW- and E–W-trending faults and

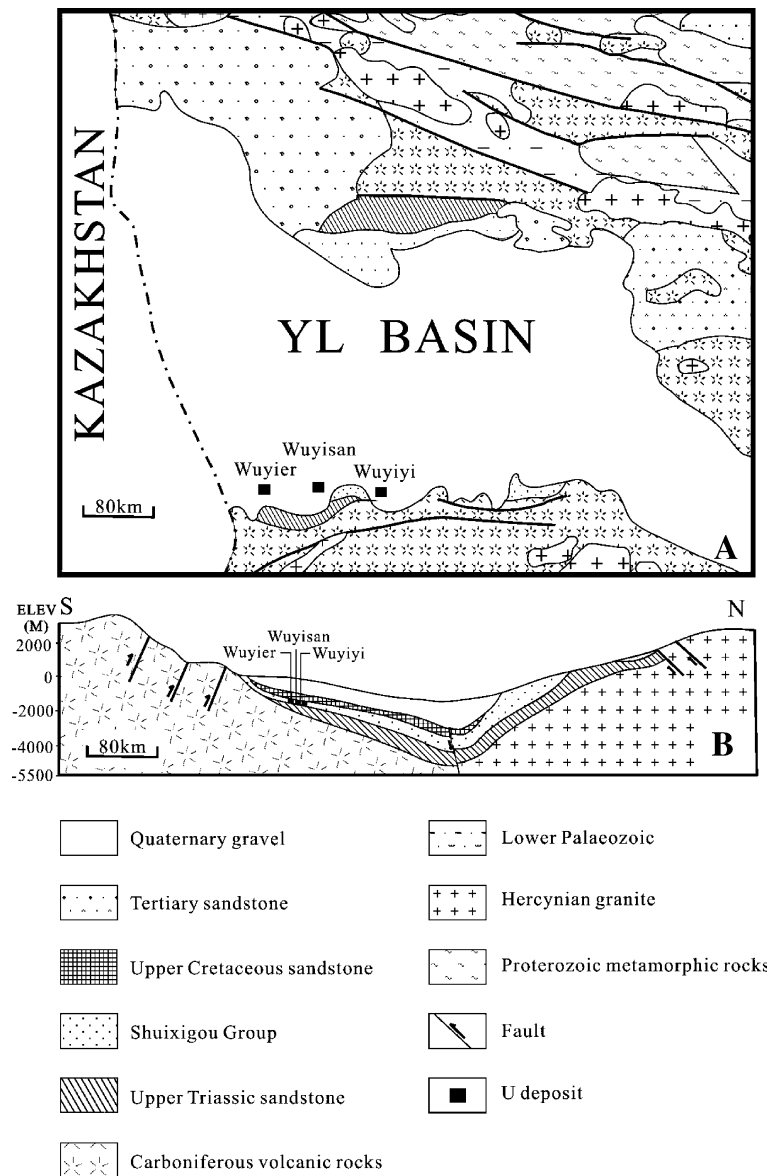


Fig. 2. Simplified maps showing regional geological setting (A) and geological cross-section (B) of the Wuyier, Wuyisan, Wuyiyi uranium district in the YL Basin (modified after 216 Geological Party, 1997).

fracture zones traverse the region and bound the two basins. Thus, the YL Basin has a NW–SE trend, whereas the Tuha Basin has an E–W trend. Both basins are elongated, closed, continental basins and host to several large oil and natural gas reservoirs, as well as coalfields. Aiting Lake located in the Tuha Basin (Fig. 3A), with an elevation of  $-155$  m, is the lowest point of elevation in continental China.

The basement and cap rocks for both the YL and Tuha basins are very similar (Figs. 2B and 3B). Basement rocks of the YL Basin are Proterozoic metasedimentary rocks, Carboniferous intermediate-acidic volcanic and volcanoclastic rocks, and granites of Hercynian age. The Tuha Basin basement rocks are Proterozoic metasedimentary units and Carboniferous intermediate-acidic volcanic and volcanoclastic rocks. The cap rocks for both basins are Triassic sandstone and shale, Jurassic conglomerate, sandstone, shale and coal, Cretaceous red conglomerate and sandstone, Tertiary red conglomerate, sandstone and shale, and Quaternary gravel, sand and clay. Lower Permian sandstone and shale only occur in the Tuha Basin.

Several unconformities separate the stratigraphic units that comprise the basin in the vicinity of the Wuyier–Wuyisan–Wuyiyi ore district. The oldest rocks exposed in this region are the Middle Proterozoic quartzite, marble, and carbonaceous slates (Fig.

2A), which are unconformably overlain by the Lower Palaeozoic conglomerate, sandstone, shale and limestone. The Carboniferous intermediate-acidic volcanic, volcanoclastic rocks rest unconformably over the Lower Palaeozoic units, and are in turn unconformably overlain by the Upper Triassic Xiaouangou group. The Lower to Middle Jurassic Shuixigou Group, consisting of conglomerate, sandstone, shale and coal beds occur on top of these Triassic rocks. Tertiary red conglomerates sandstone and shale, unconformably overlying the Lower to Middle Jurassic Shuixigou Group, themselves are unconformably overlain by the gravel, sand and clay of the Quaternary. Granites of Hercynian-age also occur in this region.

The rocks exposed in the Shihongtan ore district are similar to those in the Wuyier–Wuyisan–Wuyiyi ore district (Fig. 3), including surface exposures of Permian sandstone and shale. Several NW-, NE- and less commonly E–W-trending regional faults occur in both districts (Figs. 2 and 3).

The ore deposits are located in the southwest limb of both basins (Figs. 2 and 3), and occur within the lower to middle units of the Jurassic Shuixigou Group (Fig. 4). Ore-bearing rocks of the Jurassic Shuixigou Group dip to the northeast. The thickness of the Shuixigou Group ranges from 223

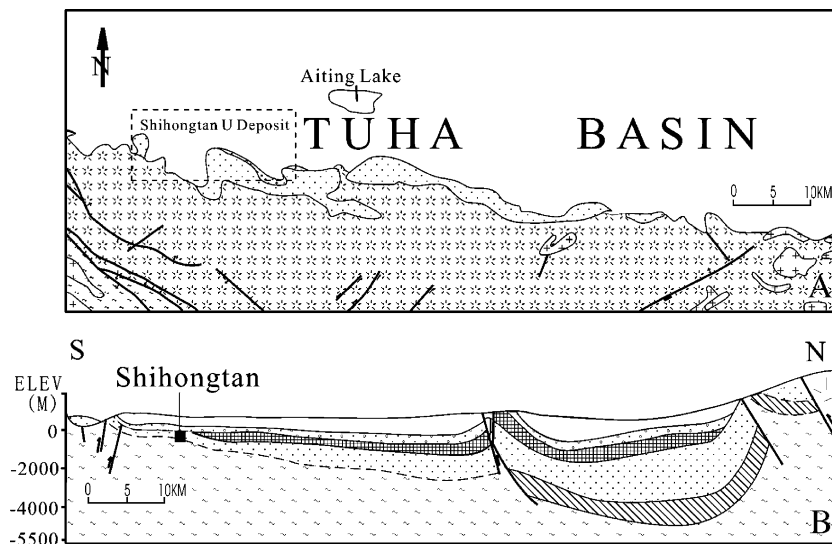


Fig. 3. Simplified maps showing regional geological setting (A) and geological cross-section (B) of the Shihongtan U-district in the Tuha Basin (modified after Northwest Institute of Uranium Geology, 1997). Symbols are the same as in Fig. 2.

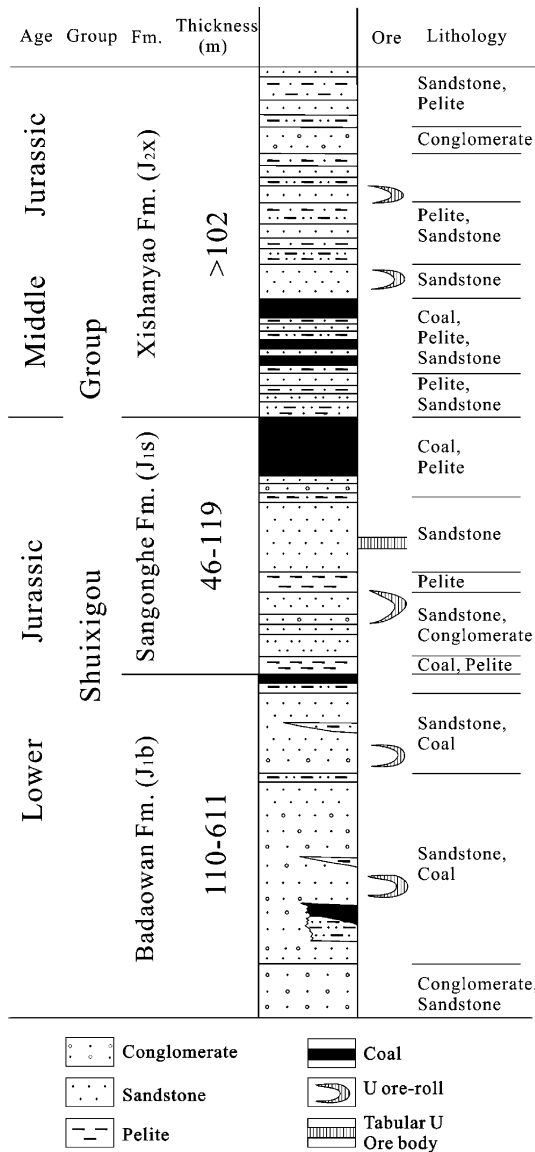


Fig. 4. Stratigraphic column of the Lower to Middle Jurassic in the YL Basin, NW China (modified after 216 Geological Party, 1997).

to 437 m in the Wuyier, Wuyisan, and Wuyiyi ore districts and 600 to 700 m in the Shihongtan ore district. The Shuixigou Group is divided into three members; starting from the bottom, these are (1) the Badaowan Formation (J<sub>1b</sub>), which lies unconformably over the Xiaoquanguou Group (Middle–Upper Triassic) in the YL Basin and over the Dikaner Formation (Middle Carboniferous) in the

Tuha Basin, (2) the Sangonghe Formation (J<sub>1s</sub>), which lies above the Badaowan Formation, and (3) the Xishanyao Formation (J<sub>2x</sub>), which lies above the Sangonghe Formation and contains most of the uranium ore of the Shihongtan deposit. A Lower Cretaceous unit overlies the Xishanyao Formation. Uranium-mineralized intervals in both basins occur at five distinct stratigraphic horizons (Fig. 4), all of which follow the inner margin of the basins.

### 3. The sandstone host rock

The sandstones hosting the U-deposits are part of the Lower to Middle Jurassic Shuixigou Group. The sandstone is gray to dark-gray, medium- to coarse-grained and contains 2% to 3% carbonaceous debris. The gently dipping (5° to 10°) ore-bearing sandstones are bounded above and below by impermeable shale. The Shuixigou Group consists of rhythmically layered grayish-green conglomerate, medium- to coarse-grained sandstone, mudstone, shale, and coal. In the southern and western regions of the Xinjiang U-province, the Shuixigou Group sandstones are important because they host the U-deposits and may partially be the U source in both districts because they are rich in U (average 9 ppm; Northwest Institute of Uranium Geology, 1997) and potassium feldspar.

The sandstone facies for both basins are interpreted to be alluvial fan-braided river facies, consisting of equal amounts of quartz, feldspar and rock fragments. The host sandstone is a piedmont alluvial fan and braided stream system, >100 km long and up to 20 km wide, covering an area exceeding 1500 km<sup>2</sup> along an E–W trend in both ore districts (Figs. 2A and 3A). The primary source of sediments was likely Proterozoic meta-sediments, Carboniferous volcanic rocks and Hercynian granites on the basin margins.

Based on a conventional classification scheme, the host sandstone is classified predominately as lithic subarkosic sandstone. No significant differences were found in sandstone mineralogy between ore and non-ore samples. Principal detrital grains in the host sandstone are composed of quartz (30% to 40%), feldspar (15% to 20%), carbonaceous debris (2% to 3%; Table 1) and rock fragments (20% to

Table 1  
Electron probe microanalyses (wt.%) of carbonaceous debris (CD) from the Wuyisan deposits

Composition	CD-1	CD-2	CD-3	CD-4	CD-5	CD-6
Al <sub>2</sub> O <sub>3</sub>	0.01	0.01	0.04	0.02	0.01	0.01
K <sub>2</sub> O	0.03	0.01	0.01	0.01	0.02	0.01
CaO	19.47	1.28	1.39	1.26	0.39	2.55
FeO <sup>a</sup>	0.60	0.03	0.03	0.02	0.07	0.05
SeO <sub>2</sub>	–	0.02	–	–	0.01	–
MoO <sub>2</sub>	0.01	0.01	–	0.01	0.02	0.04
ReO <sub>2</sub>	–	0.20	–	–	–	0.34
PbO	–	–	–	0.08	0.04	–
ThO <sub>2</sub>	–	–	0.01	–	0.01	0.02
U <sub>3</sub> O <sub>8</sub>	–	0.02	0.01	0.01	0.02	0.01
S	0.03	0.28	0.30	0.30	0.68	3.67
Total	20.15	1.86	1.79	1.71	1.27	6.70

“–”, Below detection limit (0.01%).

<sup>a</sup> Total Fe as FeO.

40%). The rock fragments consist of tuff, andesite, granite, rhyolite, quartzite, sandstone, siltstone and slate. In addition, there are minor detrital grains of biotite, muscovite, tourmaline, hornblende and heavy minerals (zircon, apatite, magnetite, allanite, monazite, sphene, ilmenite and occasionally brannerite). The detrital grains are angular to sub-angular in shape (Fig. 5A). Size sorting of the detrital grain is generally poor, indicating rapid deposition. The matrix materials of the host sandstone are clays, silt and fine-grained sand. In some deposits, such as the Wuyisan and Wuyiyi, reddish host sandstone is bleached in the vicinity of the ore. Ferric iron has been leached from the bleached sandstone and organic matter has been oxidized. It is likely that microorganisms oxidized the organic matter by reducing Fe(III) (Lovley et al., 1991).

#### 4. Ore-stage and uranium mineralization

Uranium deposits of the type that occur in the YL and Tuha continental basins are similar with respect to morphology and mineralogy. Uranium ore bodies formed where an abrupt change in redox conditions occurred. On the up-dip side of the roll- and tabular-shaped ore body, the host sandstone is yellowish orange to reddish, is devoid of pyrite, and contains little carbonaceous debris. This is likely due to the oxidation of organic matter and pyrite. These oxidized tongues of sandstone can

extend for tens of kilometers. Some of uranium ore bodies occur along single or double C-shaped roll-type surfaces or envelopes that represent interfaces between oxidized-altered rock and reduced-unaltered rock. Oxidized-altered rock lies inside the envelopes and is generally coincident with the more permeable parts of the host sand bed.

Samples containing ore-stage minerals are gray, dark gray or black in color, resulting from the occurrence of U-minerals, Fe-sulfides and carbonaceous debris. In general, the upper and lower surfaces of the envelopes are poorly mineralized, while major ore bodies occur along the lateral and terminal edges of the envelopes where they cross bedding planes in curving roll shapes. The richest U-ore, is often associated with Mo and V, and is commonly found in sharp contact with barren altered rock, where grade gradually decreases. Orebodies also occur along the envelope between the rolls, and double roll-like ore bodies. Most of the orebodies have a roll-like shape, and are 4 to 10 m in thickness and as much as 50 m in length. The tabular ore bodies have a thickness ranging from 3 to 18 m and are as much as 200 m in length; they are usually nearly parallel to bedding.

The majority of the U-mineralization in these deposits occurs within sandstone, although a minor amount of U also exists within mudstone and coal, where U is generally intermixed with carbonaceous debris and mainly occurs as unidentified, fine-grained or cryptocrystalline urano-organic complexes. Uraninite and coffinite may also be present in these ores. Plant material may contain several percent U, with minor Se, Mo and Re (Min et al., 2001; Table 1). Organic matter may play a critical role in formation of these deposits, because organic matter may be the initial reductant that reduces sulfate to sulfide, forming pyrite (Spirakis, 1996), which in turn forms the redox front that precipitates the U-ore.

Field and mineral observations suggest that U-mineralization occurred long after deposition of the Jurassic Shuixigou Group. This is likely because the mineralization occurs at the interface between oxidized and reducing facies within the sandstones. The deposits are commonly of low-grade and only occasionally are medium- to high-grade. The U-mineralization has young U–Pb ages,

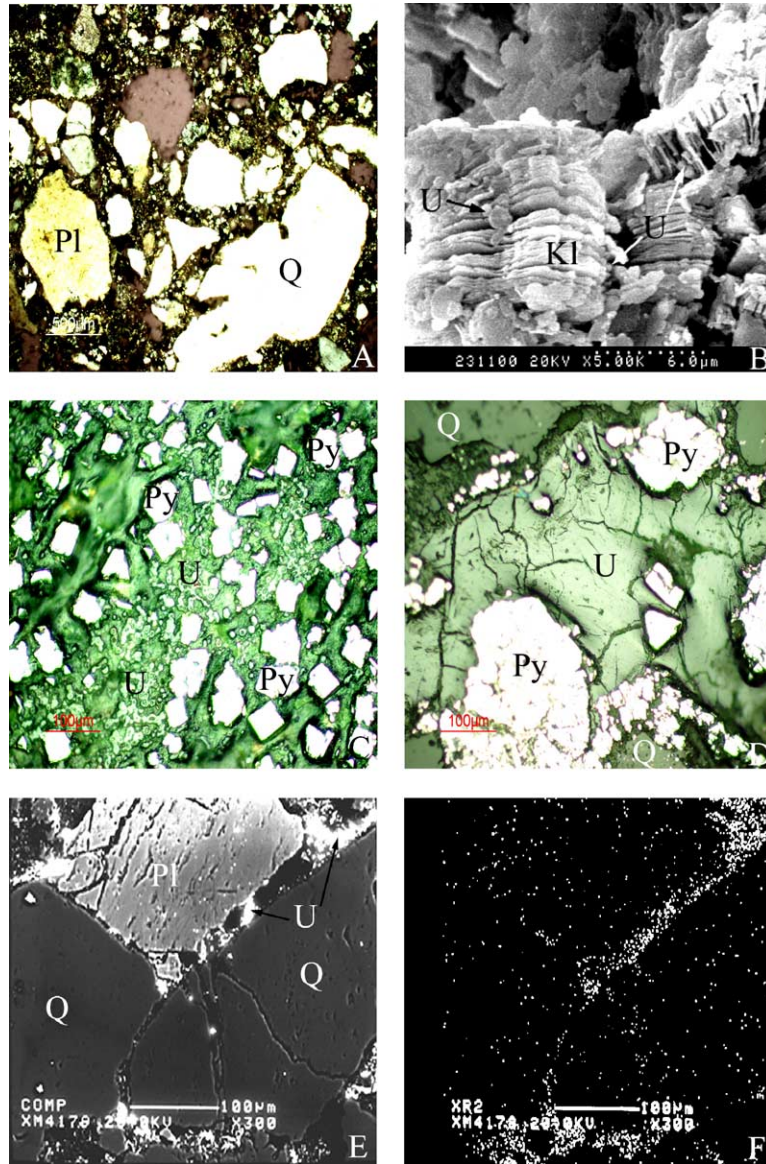


Fig. 5. Photomicrographs showing (A) Coarse- to medium-grained sandstone showing an angular to sub-angular, poorly-sorted detrital grains and corroded quartz (Q; transmitted light, crossed nicols, Wuyisan deposit). Pl: feldspar; (B) monomineralic book-like aggregates of kaolinite composed of euhedral crystals and microspherules ( $\sim 0.2$  to  $0.4 \mu\text{m}$  across) of uraninite in interstitial pore spaces of the euhedral plate crystals (back-scattered electron image, Wuyiyi deposit); (C) ore-stage euhedral pyrite (Py) and surrounding uraninite (U) with concentric colloform textures (reflected light, Shihongtan deposit); (D) massive uraninite (U), with shrinkage cracks, ore-stage pyrite cements (Py) and detrital grains in the host sandstone (reflected light, Shihongtan deposit); (E) secondary electron image of disseminated, microspherical uraninite (U) in a matrix of the host sandstone (Wuyier deposit). Pl—feldspar; Q—quartz; (F) an X-ray elemental map of the image in (E), showing the distribution of uranium.

ranging from  $11.7 \pm 0.3$  Ma to  $15.8 \pm 0.4$  Ma (Min et al., 2001), corresponding with the Himalayan (Late Tertiary) tectonism that affected a vast region of NW China.

## 5. Sampling and analytical techniques

150 samples were prepared from diamond drill cores. Optical microscopy, the electron microprobe,

scanning electron microscopy (SEM), and scanning transmission electron microscopy (STEM) were used to examine polished thin sections to determine mineral paragenesis and textures. Electron microprobe analyses were made using a JEOL JXA-8000-mode instrument at the State Key Laboratory of Mineral Deposit Research, Nanjing University. A 20 kV accelerating voltage and  $2 \times 10^{-8}$  A beam current were used. Standards used were natural uraninite for U, Th, and Pb, hornblende for K and Ca and synthetic materials for Mg, Fe, and Si. SEM investigations were made using a JEOL JSM-5800LV instrument with X-ray energy spectra analyzer at Department of Earth and Planetary Sciences, University of New Mexico, USA, as well as a Hitachi X650 SEM with X-ray energy spectra analyzer at the Center of Material Analyses, Nanjing University. STEM analyses on the uraninite were obtained using a JEOL JEM-2000FX instrument with NORAN energy dispersive X-ray spectroscopy system at Department of Earth and Planetary Sciences, University of New Mexico, USA.

To determine the clay mineralogy, clay minerals of  $<2 \mu\text{m}$  fraction were separated from the crushed sandstone samples by conventional sedimentation and centrifugation techniques, and then smeared onto glass slides. Randomly oriented powders of clay samples were analyzed by X-ray diffraction (XRD) using a Philips PW1710 diffractometer (Ni-filtered  $\text{Cu-K}\alpha$  radiation) at the State Key Laboratory of Mineral Deposit Research, Nanjing University.

## 6. Mineralogy

### 6.1. Non-metallic minerals

The most abundant non-metallic minerals in the ores are quartz, feldspar, clay, with minor amounts of calcite, siderite, mica and heavy minerals. Quartz is the most abundant detrital mineral in the sandstone. However, quartz also occurs as an alteration product of volcanic glass and as local quartz overgrowths. Quartz grains are commonly corroded (Fig. 5A) and authigenic quartz overgrowths are extensive. Hansley and Spirakis (1992) proposed that during advanced diagenesis, organic acids are produced from the humate in the sandstone. These organic acids locally dissolved quartz grains at near-neutral pH and formed silica

complexes. Some of the quartz overgrowths have sutured or irregular grain boundaries suggesting that they formed prior to major compaction (Northrop and Goldhaber, 1990). Distal sources of silica include quartz and other silicate minerals.

All feldspars, including K-feldspar and plagioclase, are clastic with anhedral–subhedral, and occasionally euhedral, shapes. Plagioclase is the most abundant and ranges in composition from andesine to oligoclase. K-feldspar is composed of perthite and microcline with lesser amounts of orthoclase. Perthite is quantitatively more abundant than microcline and orthoclase.

X-ray diffraction data show that the clay minerals in the four deposits consist of kaolinite, illite/smectite, montmorillonite and chlorite/smectite (Table 2). The content of clays in the mineralized sandstone ranges from 5.0 to 21.3 wt.%. Clay minerals in the deposits can be divided into two types: detrital or allogenic, and authigenic. Detrital clays occur in discrete clots of approximately the same size as adjacent rock fragments, quartz and feldspar grains, and have distinct outlines. Textural evidence indicates that the dominant clay mineral now present in the mineralized sandstone occurs as a pore-lining and pore-filling phase and therefore is authigenic, formed from the alteration of detrital clasts. Authigenic kaolinite generally appears as book-like aggregates (Fig. 5B) and is not only a pore-filling phase but also replaces feldspar (Lanson, 2002). Kaolinite that originated from the destruction of detrital minerals is characteristically fine-grained, coats grains, and fills the matrix of the host sandstone (Adams et al., 1978). Authigenic clay minerals in the deposits are interpreted to have formed at three different times, in response to three chemically distinct fluid events (Northrop and Goldhaber, 1990). The first authigenic clay mineral is mixed layer illite–smectite. The second authigenic clay mineral is mixed layer chlorite–smectite. Textural evidence indicates that the chlorite–smectite, which occurs only within mineralized intervals, formed at the expense of the authigenic illite–smectite. The last authigenic clay mineral is pore-filling kaolinite. Uranium minerals occasionally occur in large pores between platelets of kaolinite (Fig. 5B).

The predominant type of organic matter in the mineralized sandstone is coal, derived from detrital plant debris. Petrographic study shows that the plant debris has retained its original cellular structures.

Table 2  
Mineral compositions (in wt.%)<sup>a</sup> of clay in the four sandstone-hosted roll-type U-deposits

Sample no.	Clays <sub>total</sub>	Mont.	Illite/smectite	Kaolinite	Chlorite/smectite
<i>Wuyier</i>					
E-01	8.25	26.3	44.2	14.2	15.2
E-02	7.00	21.2	27.4	25.3	26.1
E-03	6.50	16.1	17.5	31.3	35.2
<i>Wuyisan</i>					
S-01	7.0	8.6	61.3	15.4	14.7
S-02	8.5	26.3	18.7	42.2	12.8
S-03	5.0	8.6	72.8	6.4	12.2
S-04	10.0	18.4	27.1	20.5	34.1
S-05	8.3	8.6	71.4	8.7	10.4
S-06	13.5	34.2	26.9	20.6	18.3
S-07	13.0	8.1	31.2	25.1	35.7
S-08	7.5	8.4	75.7	6.4	9.4
<i>Wuyiyi</i>					
Y-01	19.7	0.8	11.4	73.2	14.6
Y-02	20.5	1.9	11.0	72.6	14.5
Y-03	17.1	0.5	23.3	63.5	12.7
Y-04	19.4	1.8	9.6	73.8	14.8
Y-05	15.3	3.0	3.4	78.0	15.6
Y-06	15.2	4.3	22.3	60.4	13.0
Y-07	18.6	0.8	17.2	68.3	13.7
Y-08	21.3	1.3	2.9	79.8	16.0
<i>Shihongtan</i>					
H-01	5.6	30.4	15.5	54.1	–
H-02	7.9	43.0	16.6	40.4	–
H-03	6.5	57.6	12.3	30.1	–
H-04	5.6	33.2	18.3	48.5	–
H-05	5.0	49.4	13.3	37.3	–
H-06	8.3	63.3	12.4	24.3	–
H-07	6.9	36.1	19.2	44.7	–
H-08	6.7	33.0	29.4	37.6	–

“–”, Not present.

<sup>a</sup> By X-ray diffraction (XRD) analyses.

Vitrinite is the dominant form of organic matter and exhibited cellular structures, ranging from well-defined cell outlines to highly-deformed cellular textures. The primary U-minerals, uraninite and coffinite, commonly fill the cellular structures.

## 6.2. Ore minerals

The dominant U-minerals in all four deposits are uraninite and coffinite. Sulfides that occur with the uranium mineralization are pyrite, marcasite, sphalerite and less commonly galena.

### 6.2.1. Uraninite ( $m\text{UO}_2 \cdot n\text{UO}_3$ , or $\text{UO}_{2x}$ )

Uraninite is economically the most important ore mineral in all four deposits. It occurs as interstitial cement among rock fragments, disseminated grains in matrix materials (Figs. 5C–F and 6A), or fills cleavages and microfractures of pyrite, quartz, feldspar, and debris (Fig. 6B,C). Uraninite veins are commonly less than 0.1 mm wide. In some cases, micro-massive uraninite exhibits colloform textures with associated concentric banding and radial fracturing (Figs. 5C,D and 6A,D). Disseminated, microspherical uraninite, ranging from 0.2 to 0.3  $\mu\text{m}$  in diameter, is the most common morphological form and appears in cleavages of feldspar and biotite, and on clast surfaces. In higher-grade ore, disseminated, microspherical uraninite usually forms clusters where individual grains coalesce (Figs. 6E,F and 7A). Uraninite also fills micropores within clays (5B), (Fig. 7B,C), and fossilized wood cells (Fig. 7D–F). Abundant fossilized wood in the host sandstone is mineralized by uraninite and coffinite, which define the fossilized wood cell texture (Min et al., 2001). Uraninite often replaces fossilized wood (Fig. 8A), occurs along the margins of biotite grains (Fig. 6B), and occasionally pseudomorphs fossilized wood (Fig. 8A) and other minerals (Fig. 6B).

Chemical compositions of uraninite from the Wuyier, Wuyisan, Wuyiyi, and Shihongtan deposits are shown in Table 3. Analytical data show that U contents of the uraninite range from 81.09% to 85.43%, with minor impurities of Si, Al, K, Fe, Mg and Ca, and associated elements Mo, Se and Re. Uraninite from high-grade ores has rather pure chemical compositions.

### 6.2.2. Coffinite ( $\text{USiO}_4 \cdot n\text{H}_2\text{O}$ )

Coffinite is rarely documented in roll-front type U-deposits in NW China, because of its low modal abundance, minute grain size (<1  $\mu\text{m}$ ) and the fact that coffinite may be mistaken for uraninite. Therefore, very little is known about crystal habit, textural relationships with uraninite, or chemical composition. Coffinite usually occurs in high-grade ores associated with fossilized wood. Typically, coffinite occurs as euhedral tetragonal dipyrnidal crystals, which commonly form complexly interpenetrating twinned aggregates (Fig. 7E,F). It is also intergrown with uraninite within fossilized wood cells. Chemical

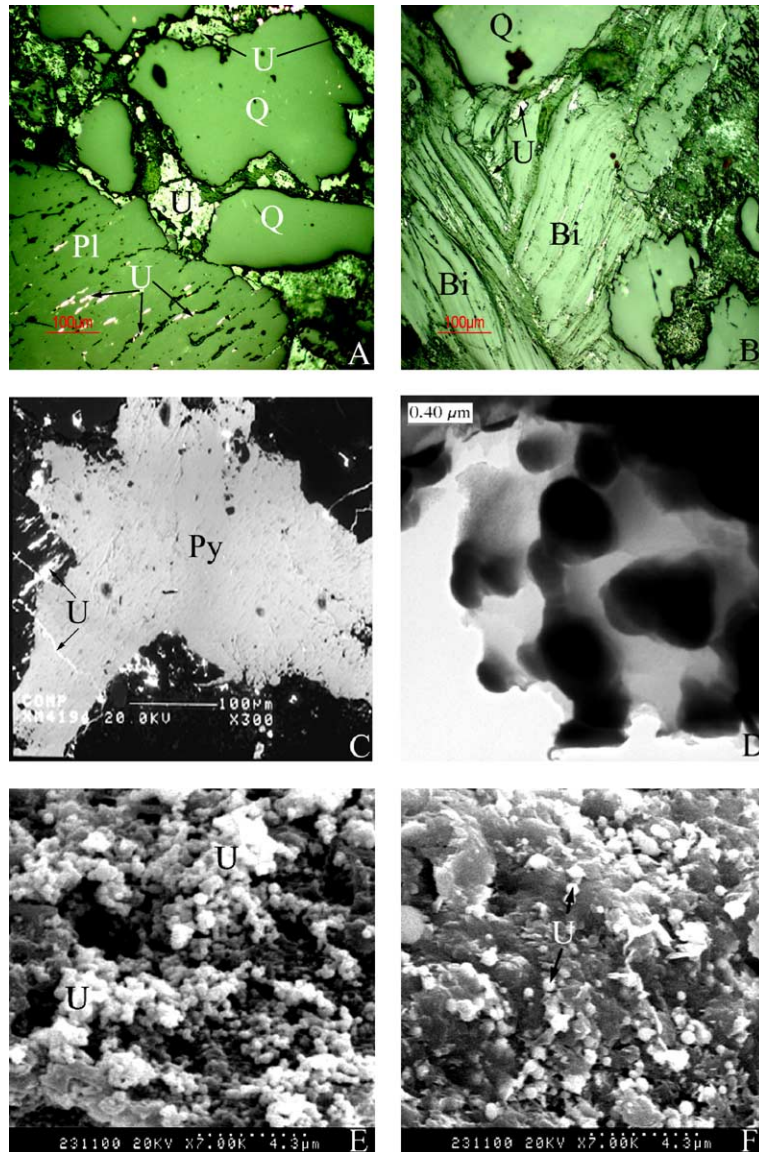


Fig. 6. Photomicrographs showing (A) disseminated grains of uraninite (U) in a matrix of sandstone, filling cleavages of detrital feldspar (Pl; reflected light, Shihongtan deposit). Q—quartz; (B) uraninite (U) filling cleavages of detrital biotite (Bi; reflected light, Shihongtan deposit). Q—quartz; (C) a micro-vein (coalesced individual microspherules) of uraninite (U) in ore-stage pyrite (Py) and uraninite along cleavages of detrital feldspar (black, left; secondary electron image, Wuyiyi deposit); (D) microspherules of uraninite (black) in a matrix of the sandstone (bright-field image of TEM, Wuyier deposit). (E) Microspherules (~0.2 to 0.4  $\mu\text{m}$  across) of uraninite (U) growing on the surface of various detrital-minerals in the sandstone (back-scattered electron image, Wuyisan deposit); (F) microspherules (~0.2 to 0.4  $\mu\text{m}$  across) of uraninite (U) growing on the surface of various detrital minerals in the sandstone (back-scattered electron image, Wuyier deposit).

analyses indicate that U and Si contents in coffinite range from 68.73% to 81.64%, and from 17.90% to 21.34%, respectively, with trace Al, Ca, Fe, Pb and S (Table 4).

Brookins (1976) showed that, at low temperatures, coffinite would only form if the activity of free silica were very high. Experiments by Goldhaber et al. (1987) indicated that  $\text{H}_2\text{S}$  would only reduce U at

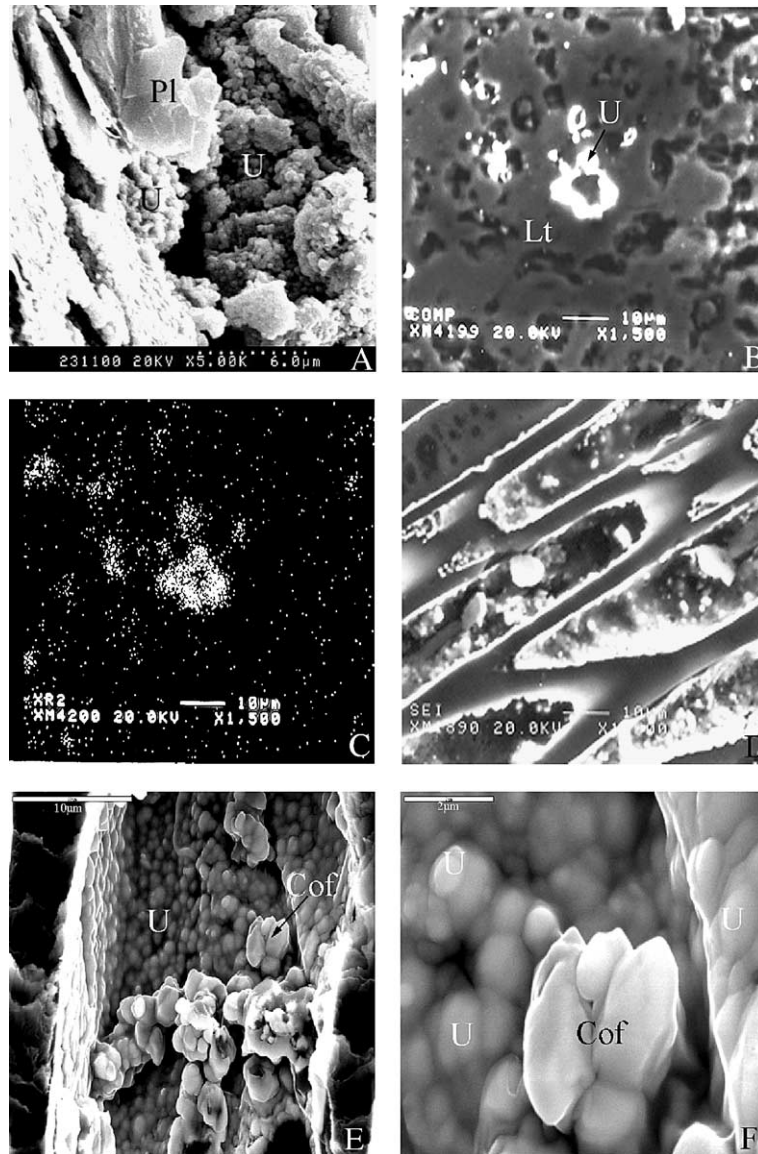


Fig. 7. Photomicrographs showing (A) microspherules ( $\sim 0.2$  to  $0.4 \mu\text{m}$  across) of uraninite on the surface of various detrital minerals and within interstitial pore spaces between feldspar (Pl; back-scattered electron image, Wuyier deposit); (B) uraninite (U) filling micropores within sandstone (secondary electron image, Wuyiyi deposit); (C) a uranium X-ray emission image of (B). (D) Uraninite microspherules (light white) and detrital minerals (dark gray) in fossilized wood cells (back-scattered electron image, Wuyiyi deposit); (E) coffinite (Cof) and microspherical, botryoidal and crustal uraninite (U) in fossilized wood cells (back-scattered electron image, Wuyisan deposit); (F) two euhedral, tetragonal dipyramid-like coffinite crystals (Cof) ( $1\text{--}2 \mu\text{m}$  across) in a fossilized wood cell, surrounded by uraninite (U; back-scattered electron image, Wuyisan deposit).

higher concentrations than those expected in nature. Some studies have suggested that the ubiquitous occurrence of organic matter with coffinite indicated a genetic link (Hansley and Fitzpartick, 1989;

Spirakis, 1996). With bacteria as a catalyst, organic matter can reduce U directly from solutions with naturally occurring concentrations (Lovley et al., 1991), which obviates the need for preconcentration

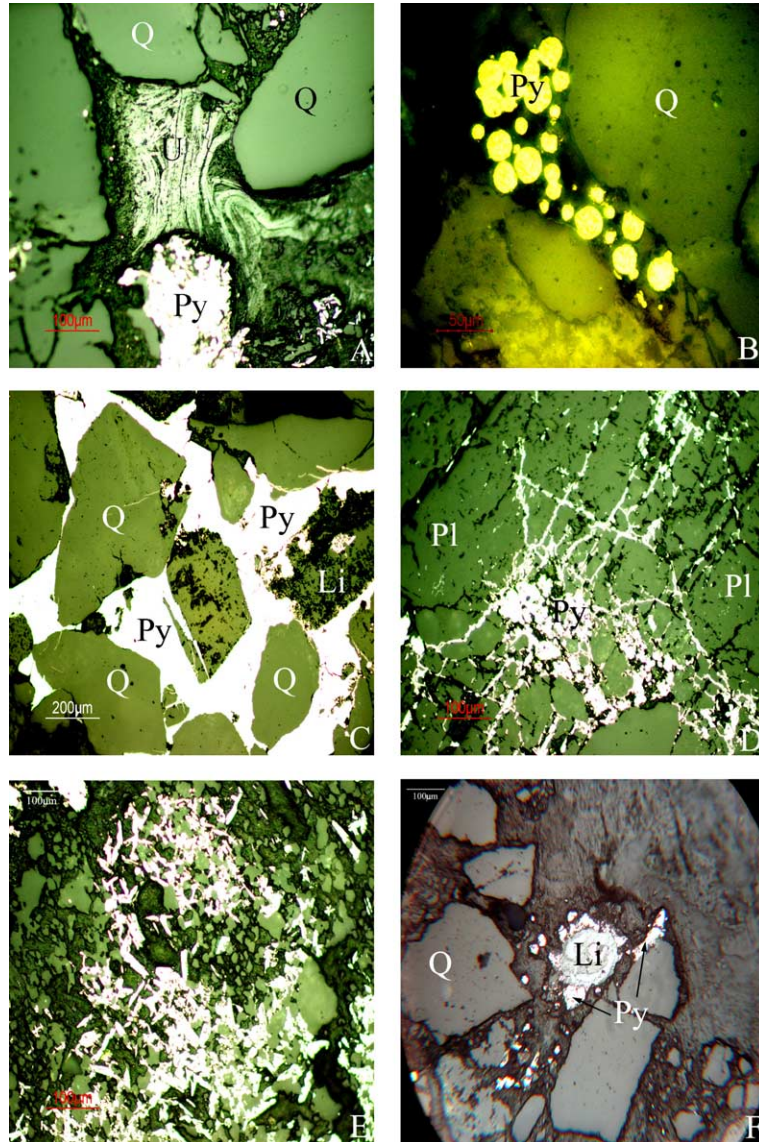


Fig. 8. Photomicrographs showing (A) uraninite (U) pseudomorphically replacing fossilized wood fragments (reflected light, Shihongtan deposit). Py—pyrite; Q—quartz; (B) framboidal pyrite (Py) in a matrix of the host sandstone (reflected light; Wuyisan deposit). Q—quartz; (C) ore-stage coarse-grained pyrite cement associated with detrital quartz (Q) and feldspar (Pl; reflected light, Wuyier deposit); (D) micro-veins of pyrite (bright white) filling cleavages and interstitial voids between detrital feldspar (reflected light, Shihongtan deposit); (E) ore-stage spindle-shaped marcasite (white) associated with the ore-stage pyrite (white; reflected light, Shihongtan deposit); (F) ore-stage pyrite (Py) rim on limonite (Li; reflected light, Shihongtan deposit). Q—quartz.

by adsorption or reduction by  $H_2S$ . Partly dissolved quartz grains in the ores provide a likely source of silica, and organo-silica complexes might provide the high silica activity needed to form coffinite (Bennett and Siegel, 1987).

### 6.2.3. Pyrite ( $FeS_2$ )

Pyrite is the dominant pre-ore sulfide in the host sandstone. Both biogenic and non-biogenic models for the genesis of these deposits require the presence of pyrite in the host rock prior to mineralization (e.g.,

Table 3  
Electron probe microanalyses (wt.%) of uraninite from the sandstone-hosted roll-type U-deposits

Sample no. <sup>a</sup>	1	2	3	4	5	6	7	8	9	10	11
K <sub>2</sub> O	0.34	0.08	0.24	0.23	0.32	0.51	0.48	0.39	0.17	0.15	0.32
SiO <sub>2</sub>	2.30	3.08	2.66	3.15	2.45	2.41	1.43	2.86	1.77	4.11	3.03
Al <sub>2</sub> O <sub>3</sub>	0.18	0.19	0.01	0.46	0.34	0.32	0.37	0.22	0.06	0.21	0.05
U <sub>3</sub> O <sub>8</sub>	83.20	85.37	82.46	81.09	81.76	83.48	85.23	84.45	85.36	83.58	85.43
CaO	3.37	3.13	4.07	4.32	4.25	4.27	2.11	1.46	2.37	3.28	4.21
FeO <sup>b</sup>	0.40	0.35	0.32	0.32	0.36	0.28	0.34	0.28	0.33	0.51	0.17
SeO <sub>2</sub>	0.02	–	0.12	0.21	–	0.18	–	0.22	0.16	0.08	0.15
ReO <sub>2</sub>	0.10	0.08	–	0.23	0.20	0.14	0.06	–	0.16	0.32	0.13
MoO <sub>3</sub>	–	0.12	0.20	0.07	0.31	0.24	0.05	0.14	0.26	–	0.32
MgO	0.13	0.05	0.08	0.08	0.14	0.21–	0.14	0.06	0.12	0.11	0.20
Total <sup>c</sup>	90.04	92.45	90.16	90.16	90.13	92.04	90.21	90.08	90.76	92.35	94.01

“–”, Below detection limit (0.01%).

<sup>a</sup> Samples from: nos.1–3, Wuyier deposit; nos.4–5, Wuyisan deposit; nos.6–8, Wuyiyi deposit; nos.9–11, Shihongtan deposit.

<sup>b</sup> Total Fe as FeO.

<sup>c</sup> Low total compositions, ranging from 90.04 to 94.01%, result from high H<sub>2</sub>O contents in the mineral, which formed under a normal or low temperature condition of 30–50 °C (Min, 1991).

Granger and Warren, 1969). Pre-ore pyrite occurs as scattered detrital euhedral, subhedral and anhedral crystals that formed prior to transport and deposition of the debris, and as authigenic framboidal pyrite, ranging in size from 0.01 to 0.04 mm in diameter (Fig. 8B), or as microscopic, euhedral–anhedral crystals (<0.1 mm) scattered in matrix of the host sandstone. Clear evidence for early diagenetic pyrite is found in rip-up clasts that are incorporated into sandstone and that typically contain small euhedral pyrite crystals, in part, associated with detrital organic debris. Other forms of pre-ore pyrite are those associated with detrital plant material; replace detrital Fe–Ti-oxide minerals and large disseminated nodules in the host sandstone.

Iron sulfide minerals (pyrite and marcasite) are important components of the geochemical systems that govern the formation of sandstone-hosted roll-front U-deposits. In the ore-rich samples, Fe-sulfides are intergrown with and surrounded by uraninite. The observation that FeS<sub>2</sub> phases are surrounded by, intergrown with, and in turn enclose U-minerals in ore zones is evidence that FeS<sub>2</sub> deposition is coeval with U-mineralization (Fig. 5C,D). Grains of ore-stage pyrite, which range from 0.05 to 0.2 mm across, are generally larger than that of pre-ore pyrite (<0.01 to 0.04 mm across; Figs. 6C, 8C,D). Ore-stage pyrite occurs as euhedral cubes, subhedral to anhedral crystals aggregates, interstitial cement surrounding detrital framework grains, and as partial replacements

Table 4  
SEM-EDS analyses (wt.%; normalized to 100%) of coffinite from the sandstone-hosted roll-type U-deposits, NW China

Sample no. <sup>a</sup>	1	2	3	4	5	6	7	8
SiO <sub>2</sub>	18.01	17.90	18.25	18.11	20.34	20.40	21.34	20.61
Al <sub>2</sub> O <sub>3</sub>	0.15	0.18	0.15	0.12	1.56	0.87	2.43	1.88
U <sub>3</sub> O <sub>8</sub>	81.48	81.64	81.15	81.37	68.73	73.25	72.80	75.43
CaO	0.20	0.16	0.22	0.18	2.66	0.47	1.27	0.48
FeO <sup>b</sup>	0.10	0.12	0.13	0.14	–	–	–	–
PbO	0.06	–	0.10	0.08	–	–	–	–
S	–	–	–	–	6.71	5.01	2.16	1.60
Total	100.00	100.00	100.00	100.00	100.00	100.00	100.00	100.00

“–”, Below detection limit.

<sup>a</sup> Samples from: nos.1–4, Wuyisan deposit; nos.5–8, Wuyiyi deposit.

<sup>b</sup> Total Fe as FeO.

of detrital titanohematite and titanomagnetite. Pyrite is often rimmed by overgrowths of marcasite. Ore-stage pyrite also fills microfractures and micropores in debris (Fig. 8D). Ore-stage pyrite is interpreted to have formed by reduction of redistributed sulfur that was produced during the oxidation of pre-ore pyrite in the altered tongue (Dahl and Hagmaier, 1974). The ore-stage pyrite textures suggest that ore-stage pyrite postdates early diagenetic pyrite (pre-ore pyrite).

The chemical composition of pyrite is shown in Table 5. Analytical data show that the pyrite contains trace amounts of Mo, Re, Se, Pb, and U. The most likely source of these trace elements was groundwater. Saunders et al. (1997) showed a correlation between trace element concentrations in groundwater and those concentrated in ferromanganese coatings on present-day stream alluvium in Alabama, United States. Based on an experimental study, Vorlicek et al. (2004) proposed that Mo forms Mo–Fe–S cuboidal clusters in pyrite and that reduction of Mo<sup>VI</sup> must occur to stabilize these structures. In mineralizing solutions containing H<sub>2</sub>S and S<sup>0</sup>-donors (i.e., polysulfides; dissolved S<sub>8</sub>), Mo is transformed to Mo<sup>IV</sup> or Mo<sup>V</sup> polysulfide/sulfide anions. Conditions that favor incorporation of Mo by pyrite also favor pyrite growth. Although anomalous grains of pyrite adjacent to U-minerals (Py–A) contained high concentrations

of U (2.01%), no obvious differences in chemical composition occur between the pre-ore pyrite and ore-stage pyrite.

#### 6.2.4. Marcasite (FeS<sub>2</sub>)

Marcasite occurs in all four deposits, with average modal abundance ranging from 2 to 3 vol.%. Ore-stage marcasite, however, is typically less common than ore-stage pyrite. It is intimately associated with pyrite and primary U-minerals, and occurs as euhedral spindle-shaped and subeuhedral single crystals (Fig. 8E). It is abundant in high-grade ores where its abundance is ~30% of total FeS<sub>2</sub>. The abundance of marcasite sharply and systematically decreases with distance from the altered tongue. Based on textural relationships and intimate association with U-mineralization (especially high-grade ore), we speculate that ore-stage marcasite in the deposits also formed by reduction of redistributed sulfur that originated by oxidation of pre-ore FeS<sub>2</sub> during development of the altered tongue. According to Reynolds and Goldhaber (1983), formation of ore-stage marcasite may be related to mixing of two fluids; an oxidizing ground water that originated by recharge at surface, and a reducing brine, which permeated the host rocks along a fault from depth. Marcasite forms in the presence of relatively low pH (≤7.0) and elemental sulfur, while

Table 5

Electron probe microanalyses (wt.%) of pyrite (Py) and SEM-EDS analyses of sphalerite (Sh) from the sandstone-hosted roll-type U-deposits, NW China

Mineral <sup>a</sup>	Py-A	Py-B	Py-C	Py-D	Py-E	Py-F	Py-G	Py-H	Sh <sup>b</sup>
Al <sub>2</sub> O <sub>3</sub>	0.03	0.01	–	0.01	–	–	–	0.02	–
SiO <sub>2</sub>	0.07	0.01	0.01	–	–	0.01	–	0.01	–
K <sub>2</sub> O	–	0.01	0.02	0.01	–	–	–	0.01	–
CaO	0.18	0.05	0.06	0.08	0.01	–	0.01	–	–
FeO <sup>c</sup>	45.05	46.12	45.47	45.11	46.19	46.53	44.68	46.06	0.40
SeO <sub>2</sub>	–	0.01	–	–	–	–	–	0.01	–
MoO <sub>2</sub>	1.24	1.45	0.36	0.32	0.48	0.43	0.44	0.38	–
ReO <sub>2</sub>	0.17	–	–	–	0.15	–	0.47	0.04	–
PbO	0.17	0.08	0.12	0.04	–	0.14	0.04	0.05	–
U <sub>3</sub> O <sub>8</sub>	2.01	0.02	0.03	–	–	–	0.04	–	–
ZnO	–	–	–	–	–	–	–	–	33.77
S	53.54	52.00	50.40	51.56	52.90	53.83	54.07	53.17	65.83
Total	97.48	99.78	96.47	97.13	99.73	100.94	98.71	99.75	100.00

“–”, Below detection limit. As, Co and Ni were not detected.

<sup>a</sup> Samples from: sphalerite, Wuyiyi deposit; pyrite (no. Py-A~Py-H), Wuyisan deposit.

<sup>b</sup> By SEM analyses.

<sup>c</sup> Total Fe as FeO.

pyrite forms at higher pH ( $\geq 7.0$ ) in the presence of polysulfide ions (Reynolds and Goldhaber, 1983). Marcasite also occurs in the unmineralized sandstone.

#### 6.2.5. Sphalerite (ZnS) and galena (PbS)

Sphalerite is a minor sulfide occurring as a fine-grained dissemination throughout the matrix and replacing fossilized wood cells. The straw yellow anhedral grains range in size from 0.02 to 0.1 mm in diameter and are zoned. Chemical analysis (Table 5) indicates that the mineral is rather pure, with only trace amounts of Fe (0.4 wt.%). Galena is also a minor constituent of the mineralization and occurs as isolated anhedral grains (<0.1 mm across) associated with colloform uraninite. The Pb from the galena is considered to be radiogenic in origin (Min, 1991) and exsolved out from the uraninite, and is thus slightly later than the uraninite.

### 7. Texture and structure of the ores

All of the ores possess a sedimentary-like texture. For example, U-mineralization mainly occurs in the matrix of sandstone (Figs. 5C–F, 6A, 8A) where grain size ranges from 0.25 to 1.00 mm in diameter. Some detrital quartz and feldspar grains in the sandstone are corroded (Fig. 5A), especially where uraninite, coffinite and marcasite occur together.

The cells of fossilized carbonaceous debris are commonly replaced by uraninite, coffinite, pyrite, sphalerite, calcite, quartz, and clays (Fig. 7D–F). Cell sizes range from 0.02 to 0.06 mm in diameter. Uraninite and coffinite replace the cell walls of fossilized wood and a thin selvage of uraninite and coffinite outlines the cell centers (Min et al., 2001). Some samples show honeycomb-like fossilized wood cellular structures, while others show long lenticular wood cells with thick cell walls. Uraninite also pseudomorphs framboidal pyrite, chlorite, carbonized fossilized wood debris, and biotite (Figs. 6B and 8A). Uraninite and pyrite commonly occur as cements in the ore specimens (Figs. 5C,D, 8C), partially replacing matrix material in the sandstone. Colloform uraninite with shrinkage cracks also occurs as cement in the sandstone (Figs. 5C,D and 6A). Limonite also shows a colloform texture (Fig. 8F).

Euhedral, cubic crystals of pyrite are commonly observed (Fig. 5C). Ore-stage marcasite occurs as euhedral in shape (Fig. 8E). Euhedral, tetragonal dipyrarnidal-like crystals of coffinite fill cellular structures at the Wuyisan deposit (Fig. 7F). In all of the four deposits, authigenic pyrite possesses a framboidal texture (Fig. 8B). The framboidal pyrite exists commonly in the matrix of the rock and within fossilized wood cells, and along cleavages of biotite and feldspar. Its framboidal texture and close association to carbonized fossilized plant fragments indicate an in situ biogenic origin by bacterial sulfate reduction for the early diagenetic pyrite (Reynolds and Goldhaber, 1983). Bacterial metabolic processes exert fundamental controls on reactions that favor concentration of uranium. Some of the uraninite pseudomorphically replaces framboidal pyrite.

In the richer ores, grains of detrital quartz and feldspar are more fractured than those in low-grade ores. Uraninite and ore-stage pyrite fill the microfractures that occur in the detrital grains (Figs. 6C and 8D). Uraninite fills microfractures in ore-stage pyrite (Fig. 6C), suggesting that uraninite postdates some of the ore-stage pyrite. Some of the microveins occur along cleavages within detrital feldspar (Fig. 8D), or biotite (Fig. 6B). Uraninite in the richer ores often occurs as microspherical grains, ranging from 0.2 to 0.3  $\mu\text{m}$  across, within interstitial spaces between and on the surfaces of the detrital grains (Figs. 5B,E,F, 6D–F, 7A). Framboidal pyrite occurring in the matrix of the sandstone and within the fossilized wood cells also has a microspherical structure (Fig. 8B).

### 8. Assemblage and paragenetic sequence of mineral in the ores

Minerals in the ores from the four deposits can be divided into three categories: (1) detrital, (2) authigenic, and (3) ore-stage mineralization. The angular-shaped detritus, consisting of quartz, feldspar, mica, accessory minerals, rock fragments and carbonaceous debris, was deposited in the Early to Middle Jurassic and was cemented by authigenic clays, minor calcite (Table 1) and siderite (Fig. 9). Other authigenic minerals, such as pyrite, chlorite, hematite, clays, and quartz, replace detrital phases or occur as overgrowths that formed during the diagenesis of the

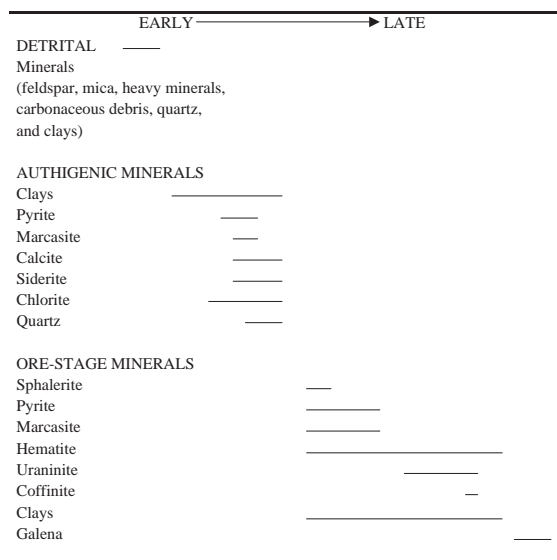


Fig. 9. Paragenetic scheme illustrating the genetic sequence of minerals associated with sandstone-hosted roll-front U-deposits, NW China.

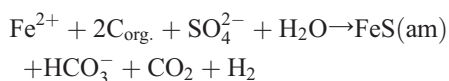
sandstone. Quartz is the most abundant authigenic mineral and occurring as overgrowths on detrital quartz and feldspar grains. The ore-stage minerals uraninite, coffinite, pyrite, sphalerite, and marcasite precipitated in the fossilized wood-cell holes and interstices of the sandstone, and replaced carbonaceous debris and matrix material during development of the altered tongue. Uraninite selectively replaced pyrite and carbonaceous debris, while coffinite primarily replaced carbonaceous debris. Precipitation of the ore-stage pyrite appears to slightly precede formation of primary U-minerals (Figs. 5C,D, 6C, 8A, 9). Galena postdates the uranium minerals and occurs in the shrinkage cracks within uraninite.

## 9. Discussion

Sandstone-hosted roll-front and tabular U-deposits are the second most economically important uranium deposit-type in the world (OECD/NEA, 1998). A genetic mechanism for sandstone-hosted roll-front U-deposits has been extensively discussed (Gross, 1956; Galloway, 1978; Reynolds and Goldhaber, 1978, 1982, 1983; Finch, 1996; Plant and Saunders, 1999). The roll-front deposits are thought to reflect dynamic

fluid flow with mass transport of U in groundwater moving down-dip within a confined aquifer in response to a hydraulic gradient. Uranium minerals precipitate at redox fronts that may be abrupt or diffuse depending on the nature, abundance and distribution of reducing agents. The typical crescent-shaped cross-section of roll-front deposits is thought to reflect the more rapid migration of groundwater through the middle layers of permeable sandstone units whereas tabular deposits, are formed by oxidizing U-bearing groundwater that enters the host sandstone from the edges of the basin (Plant and Saunders, 1999).

The precipitation mechanisms of pyrite and marcasite in sandstone-hosted U-deposits have been studied by many mineralogists (Reynolds and Goldhaber, 1978, 1982, 1983; Saunders et al., 1997; Shikazono and Utada, 1997; Shikazono and Nakata, 1999). Marcasite is metastable with respect to pyrite. Therefore, marcasite and pyrite form under different physiochemical conditions. Reynolds and Goldhaber (1978, 1983) considered that pH and the types of sulfur species are among the dominant controls governing the formation of either pyrite or marcasite. Relatively low pH (<7), with high concentrations of elemental sulfur, and low concentrations or absence of polysulfide, favor marcasite precipitation, whereas pH>7 and an abundance of polysulfide species favor pyrite formation (Korolev and Korozenko, 1965; Kullerud, 1966). Sedimentary Fe-sulfides (pyrite or marcasite) are generally considered to form from more soluble amorphous monosulfide (Schoonen and Barnes, 1991; Saunders et al., 1997). The initial iron monosulfide formation during biogenic sulfate reduction can be expressed by the reaction:



Sulfate reducing-bacterial can elevate the pH ( $\geq 7$ ) of fluids. The high polysulfide content in uranium-bearing solutions, therefore favors the precipitation of pyrite. The presence of ore-stage marcasite may be related to mixing of two fluids, an oxidizing groundwater that originated by recharge at the outcrop, and the other, a reducing brine which leaked into the host rocks along a fault from depth. The mixing of two fluids also resulted in formation of the tabular ore bodies.

In the four deposits, framboidal textures of authigenic pyrite associated with detrital plant debris, and its light sulfur isotopic composition (from 2.4‰ to –40‰) suggest a biogenic origin. For example, fifteen sulfur isotopic analysis of pyrite from the ore samples and host sandstones of the Shihongtan deposit have  $\delta^{34}\text{S}$  values between +2.4‰ and –39.2‰ (mean –8.4‰). During diagenesis of the host sandstone, scattered euhedral and subhedral pyrite was formed by extensive bacterial reduction of sulfate with concomitant oxidation of organic matter, and by hydrolysis reactions of organic matter that produced  $\text{CH}_4$  and  $\text{CO}_2$  (Shikazono and Utada, 1997). Organic matter was likely the source of nutrients for the sulfate-reducing bacteria. Saunders et al. (1997) reported similar textures and  $\delta^{34}\text{S}$  values (+3‰ to –40‰) for 1.5 cm-sized crystals of pyrite near the base of the alluvial aquifer in Alabama, USA. In addition, fossilized bacteria and algae in ore sample are mineralized with uraninite and coffinite (Min et al., 2003). In addition to the readily available biomass during the Jurassic, these types of uranium deposits formed at low temperatures (30 to 50 °C) suitable for biogenic activity. TEM analysis of uraninite shows that fossilized spores replace uraninite (Min et al., 2003). These spores were living bacteria that existed during the early to middle stages of mineralization. Therefore, microorganisms were clearly important in formation of the four sandstone-hosted roll-type U-deposits, where sulfate-reducing bacteria and other anaerobic bacteria could reduce and accumulate uranium.

Fluorescence examination of thin sections of the ores and host sandstone from the four deposits revealed that the fossilized microorganisms and associated minerals strongly fluoresce, indicating the presence of petroleum compounds, such as  $\text{CH}_3$  (Min et al., 2003). Petroleum compounds are a strong reductants for U(VI). Experimental oil–sandstone–water reactions in hydrocarbon reservoirs, performed by Shebl and Surdam (1996), showed that crude oil can reduce oxidized mineral phases. For example, Fe-oxide reduction by hydrocarbons causes oxidation of the hydrocarbons and releases  $\text{CO}_2$  and organic acids. These organic acids dissolved silicate minerals (quartz and feldspar etc.) and cements in sandstone. The original porosity of the sandstone increased by 13% to 20%.

Similar reactions may have occurred within the Jurassic sandstones of the YL Basin and Tuha Basin. Several large oil, natural gas, and coal fields occur within these basins, which likely produced organic acids that enhanced sandstone porosity and facilitated migration of the ore-bearing fluids and deposition of uranium minerals.

## 10. Conclusions

- (1) The largest U-orebodies in the Wuyier, Wuyisan Wuyiyi and Shihongtan deposits occur in permeable, medium- to coarse-grained and poorly-sorted lithic subarkosic Jurassic sandstone. The host sandstone is alluvial fan-braided river facies, and occurs as continental basin fill. The sandstone lies on Carboniferous intermediate-acidic volcanic, volcanoclastic rocks and Hercynian granites, which are considered the source of the sediments and the uranium.
- (2) Minerals associated with these deposits are broadly categorized as detrital, authigenic, and ore-stage mineralization. Detrital minerals include quartz, feldspar, mica, accessory minerals, rock fragments, carbonaceous debris, and clay. Authigenic minerals, which formed during diagenesis, are clay, pyrite, marcasite, chlorite, quartz, calcite, and siderite. Ore-stage minerals are uraninite, coffinite, pyrite, marcasite, sphalerite, galena, and hematite.
- (3) The grain size of the ore minerals is generally too small (<1–2  $\mu\text{m}$ ) to be observed with optical microscopy. Primary U-minerals occur within fossilized wood cells, interstitial spaces between cells, microfractures, and replace carbonaceous debris and matrix materials in the more permeable Lower–Middle Jurassic sandstones.
- (4) These deposits formed at the redox interface between a uraniferous oxidizing brine and a reducing environment. Carbonaceous debris, the pre-ore sulfide minerals (pyrite and marcasite) and increased permeability due to fracturing and corrosion of minerals are associated with the highest-grade ore (Gross, 1956; Shebl and Surdam, 1996).

## Acknowledgements

We are grateful to the Northwest Institute of Uranium Geology (NWIUG) and 216 Geological Party, China National Nuclear Corporation, who provided drillcores and partial unpublished data. The work was supported by the National Natural Science Foundation of China (Grant No. 40173031), Ph.D. Base Research Foundation from the Education Ministry of China (Grant No. 20020284036), and partially Division of Chemical Sciences, Geosciences, and Biosciences, Office of Basic Energy Sciences, U.S. Dept. of Energy, under contract DE-AC05-00OR22725 with Oak Ridge National Laboratory, managed and operated by UT-Battelle, LLC. The manuscript benefited considerably from critical reviews and helpful comments by N. Cook, R.I. Grauch, K. Savage, and J. Saunders.

## References

- 216 Geological Party, 1997. Geological Report of the Wuyiyi Uranium Deposit. Unpublished Geological Report (in Chinese).
- Adams, S.S., Curtis, H.S., Hafen, P.L., Salek-Nejad, H.S., 1978. Interpretation of postdepositional processes related to the formation and destruction of the Jackpile-Paguete uranium deposit, northwest New Mexico. *Economic Geology* 73, 1635–1654.
- Adler, H.H., 1964. The conceptual uranium ore roll and its significance in uranium exploration. *Economic Geology* 59, 46–53.
- Bennett, P.C., Siegel, D.I., 1987. Increased solubility of quartz in H<sub>2</sub>O due to complexing by organic compounds. *Nature* 326, 684–686.
- Brookins, D.G., 1976. Position of uraninite and/or coffinite accumulation to the hematite–pyrite interface in sandstone-type deposits. *Economic Geology* 71, 944–948.
- Chen, K.M., 1994. Formation of Petroleum and Gas in the Tuha Basin. Petroleum Industrial Publisher, Beijing. 23 pp. (in Chinese).
- Chen, Z.B., Zhao, F.M., Xiang, W.D., Chen, Y.H., 2000. Uranium province in China. *Acta Geologica Sinica* 74, 587–594.
- Dahl, A.R., Hagmaier, J.L., 1974. Genesis and Characteristics of the Southern Power River Basin Uranium Deposits, Wyoming, USA. Formation of Uranium Ore Deposits. International Atomic Energy Agency, Vienna, pp. 201–216.
- Finch, W.L., 1996. Uranium provinces of North America—their definition, distribution, and models. *US Geological Survey Bulletin* 2141, 18–30.
- Galloway, W.E., 1978. Uranium mineralization in a coastal-plain fluvial aquifer system: Catahoula Formation, Texas. *Economic Geology* 73, 1655–1676.
- Goldhaber, M.B., Hemingway, B.S., Mobagheghi, A., Reynolds, R.L., Northrop, H.R., 1987. Origin of coffinite in sedimentary rocks by a sequential adsorption–reduction mechanism. *Bulletin of Mineralogy* 110, 131–144.
- Granger, H.C., Warren, C.G., 1969. Unstable sulfur compounds and the origin of roll-type uranium deposits. *Economic Geology* 64, 160–171.
- Granger, H.C., Santos, E.S., Dean, B.G., Moore, F.B., 1961. Sandstone-type uranium deposits at Ambrosia Lake, New Mexico—an interim report. *Economic Geology* 56, 1179–1209.
- Gross, E.B., 1956. Mineralogy and paragenesis of the uranium ore, Mi Vida Mine, San Juan County, Utah. *Economic Geology* 51, 632–648.
- Hansley, P.L., Fitzpartick, J.J., 1989. Compositional and crystallographic data on REE-bearing coffinite from the Grants uranium region, northwestern New Mexico. *American Mineralogist* 74, 263–270.
- Hansley, P.L., Spirakis, C.S., 1992. Organic matter diagenesis as the key to a unifying theory for the genesis of tabular uranium–vanadium deposits in the Morrison Formation, Colorado Plateau. *Economic Geology* 87, 352–365.
- IAEA, 1996. Guidebook to Accompany IAEA Map: World Distribution of Uranium Deposits. IAEA, Vienna, pp. 20–210.
- Korolev, D.F., Korozenko, S.V., 1965. Experimental study of the formation of iron sulfides from solution. *Doklady Akademii Nauk SSSR* 165, 194–196.
- Kullerud, G., 1966. Sulfide studies. In: Abelson, P.H. (Ed.), *Research in Geochemistry*, vol. 2. John Wiley, New York, pp. 286–321.
- Lanson, B., 2002. Authigenic kaolin and illite minerals during burial diagenesis of sandstone: a review. *Clay Minerals* 37, 1–22.
- Lovley, D.R., Phillips, J.P., Gorby, Y.A., Landa, E.R., 1991. Microbial reduction of uranium. *Nature* 350, 413–416.
- Melin, R.E., 1964. Description and origin of uranium deposits in Shirley basin, Wyoming. *Economic Geology* 59, 835–849.
- Min, M.Z., 1991. Mineral paragenetic associations and textural patterns in the uranium deposits of granite-type in China. In: Cuney, M. (Ed.), *Primary Radioactive Minerals: the Textural Patterns of Radioactive Mineral Paragenetic Associations*. pp. 75–104. Theophrastus, Zographou, Athens.
- Min, M.Z., Luo, X.Z., Mao, S.L., Wang, Z.Q., Wang, R.C., Qin, L.F., Tan, X.L., 2001. An excellent fossilized wood cell texture with primary uranium minerals at a sandstone-hosted roll-type uranium deposit, NW China. *Ore Geology Reviews* 17, 233–239.
- Min, M.Z., Wang, R.C., Bian, L.Z., 2003. Biomineralization in sandstone-hosted interlayer oxidation-zone type uranium deposits. *Progress in Natural Science* 13, 164–168 (in Chinese).
- Northrop, H.R., Goldhaber, M.B., 1990. Genesis of the tabular-type vanadium–uranium deposits of the Henry basin, Utah. *Economic Geology* 85, 215–269.
- Northwest Institute of Uranium Geology, 1997. Geological report of the Shihongtan uranium deposit. Unpublished geological report (in Chinese).
- OECD/NEA, 1998. Uranium, Resources, Production and Demand 1997. OECD, Paris, pp. 12–20.
- Plant, J.A., Saunders, A.D., 1999. Uranium ore deposits. In: Burns, P.C., Finch, R. (Eds.), *Uranium: Mineralogy, Geo-*

- Chemistry and the Environment, *Reviews in Mineralogy*, vol. 38, pp. 272–319.
- Reynolds, R.L., Goldhaber, M.B., 1978. Origin of south Texas roll-type uranium deposit: II. Sulfide petrology and sulfur isotope studies. *Economic Geology* 73, 1690–1705.
- Reynolds, R.L., Goldhaber, M.B., 1982. Biogenic and nonbiogenic ore-forming processes in the South Texas uranium district: evidence from the Panna Maria deposit. *Economic Geology* 77, 541–556.
- Reynolds, R.L., Goldhaber, M.B., 1983. Iron disulfide minerals and the genesis of roll-type uranium deposits. *Economic Geology* 78, 105–120.
- Saunders, J.A., Pritchett, M.A., Cook, R.B., 1997. Geochemistry of biogenic pyrite and ferromanganese stream coatings: a bacterial connection? *Geomicrobiology Journal* 14, 203–217.
- Schoonen, M.A.A., Barnes, H.L., 1991. Reactions forming pyrite and marcasite from solution: II. Via FeS precursors below 100 °C. *Geochimica et Cosmochimica Acta* 55, 1505–1515.
- Shawe, D.R., Granger, H.C., 1965. Uranium ore rolls, an analysis. *Economic Geology* 60, 240–250.
- Shebl, M.A., Surdam, R.C., 1996. Redox reactions in hydrocarbon clastic reservoirs: experimental validation of this mechanism for porosity enhancement. *Chemical Geology* 132, 103–117.
- Shikazono, N., Nakata, M., 1999. Compositional variation of pyrite, diagenetic alteration and genesis of tonalite sandstone-type uranium deposit in Japan. *Resource Geology* 15, 55–64.
- Shikazono, N., Utada, M., 1997. Stable isotope geochemistry and diagenetic mineralization associated with the Tono sandstone-type uranium deposit in Japan. *Mineralium Deposita* 32, 596–606.
- Spirakis, C.S., 1996. The roles of organic matter in the formation of uranium deposits in sedimentary rocks. *Ore Geology Reviews* 11, 53–69.
- Vorliceck, T.P., Kahn, M.D., Kasuya, Y., Heiz, G.R., 2004. Capture of molybdenum in pyrite-forming sediments: role of ligand-induced reduction by polysulfides. *Geochimica et Cosmochimica Acta* 68, 547–556.